ChemPhysChem

Research Article
doi.org/10.1002/cphc.202400936

Chemistry Europe
European Chemical Societies Publishing

www.chemphyschem.org

Commercial Silica Materials Functionalized with a Versatile Organocatalyst for the Catalysis Of Acylation Reactions in Liquid Media

Raoul D. Brand,[a] Mareike Maass,[a] Anatoliy G. Grebenyuk,[b] Alexander A. Golub,[c] and Bernd M. Smarsly*[a, d]

Silica materials, natural and synthetic variants, represent a promising material for the application in heterogeneous organocatalysis due to their readily modifiable surface and chemical inertness. To achieve high catalyst loadings, usually, porous carriers with high surface areas are used, such as silica monoliths or spherical particles for packed bed reactors. While these commercial materials were shown to be efficient supports, their synthesis is elaborate, and thus less complex and cheaper alternatives are of interest, especially considering scaling up for potential applications. In this work, two commercial silica materials functionalized with the organocatalyst 4-(dimethylamino)pyridine (DMAP) were used in catalytic acylation reactions: a mesoporous silica gel (Siliabond-DMAP) and non-porous silica nanoparticles (Ludox). While both were successfully used in the acylation of phenylethanol, the latter required significantly longer reaction times, presumably due to the lack of mesopores and the associated spatial confinement, as well as agglomeration that limits the active amount of catalyst. Furthermore, we find that the influence of the linker molecule is negligible, since for two different linker motifs the reaction yields and activation energy remain largely similar. Lastly, as main result the commercial material Siliabond-DMAP, despite the non-uniform particles, were employed in a flow setup, thus demonstrating the potential as support material for application in heterogeneous organocatalysis.

Introduction

Porous materials play a crucial role in all fields of heterogeneous catalysis, for both inorganic as well as organic reactants, ranging from macroscopic pellets and foams in industrial size reactors to highly tuned nanoporous materials in microreactors. Spurred by the Nobel Prize in 2021 granted for the development of asymmetric organocatalysis, the immobilization of organocatalysts in a porous framework might represent a concept to further exploit the potential of organocatalysts, especially if used in liquid media. Possible benefits can be the high contact time between reactant and immobilized catalyst, as well as the increased safety and scalability of the reactors while simultaneously evading costly separation processes. As such, a number of routinely performed chemical transformations in organic synthesis may potentially be performed by heterogeneous catalysis through the functionalization of porous carrier materials with organocatalyst molecules.[1] For instance, following this concept, the well-known organocatalyst 4-(dimethylamino) pyridine (DMAP) was immobilized on both, meso-macroporous silica monoliths as well as mesoporous silica particles commonly used for HPLC applications.[2,3] Both types of materials offer beneficial properties in regards to permeability and surface area and were, for example, successfully used in acylation reactions in batch and in a flow setup. In principle, silica is a quite suitable carrier material, as various reliable synthetic concepts are available for the covalent linkage of organocatalysts and as the porosity can be deliberately designed. However, such special porous materials show a high degree of complexity and thus require costly and time-consuming syntheses, possibly preventing the scaling up of this kind of heterogeneous organocatalytic synthesis.

Hence, it would be desirable to find a readily available and commercial silica carrier material that still reaches similar performance in organocatalysis, but features a less intricate and elaborate synthesis. Therefore, in this work, our focus shifted to two different silica supports: Siliabond-DMAP and Ludox colloidal silica. The commercially available Siliabond material is described as an „irregular silica gel" by the manufacturer (Silicycle), exhibiting a large size distribution, but no uniform particle morphology. Thereby it differs from the HPLC-opti-

[a] R. D. Brand, M. Maass, B. M. Smarsly
Institute of Physical Chemistry, Justus-Liebig-University Giessen, Heinrich-Buff-Ring 17, D-35392 Giessen, Germany
E-mail: Bernd.Smarsly@phys.chemie.uni-giessen.de

[b] A. G. Grebenyuk
Department of Quantum Chemistry and Chemical Physics of Nanosystems, Chuiko Institute of Surface Chemistry of National Academy of Sciences of Ukraine, 17 General Naumov Street, 03164 Kyiv, Ukraine

[c] A. A. Golub
Department of Chemistry, National University of Kyiv-Mohyla Academy, 2 Skovoroda Street, 04070 Kyiv,Ukraine

[d] B. M. Smarsly
Center for Materials Research, Heinrich-Buff-Ring 16, D-35392 Giessen, Germany

Supporting information for this article is available on the WWW under https://doi.org/10.1002/cphc.202400936

mized LiCrospher particles used previously, also with respect to the linker through which the catalyst is immobilized is different (Figure 1). Using these Siliabond materials, we intended to clarify the role of the mesopore space and the impact of an irregular particle shape for the application in flow, as well as into the influence of the chosen linker motif. The latter is investigated in a comparative study, by functionalizing the raw silica material (Siliaflash), used for Siliabond-DMAP, *via* our previously established synthetic route.[3] Furthermore, quantum mechanical simulations for the DMAP motif immobilized by both linker molecules are performed, to gain a deeper understanding of the behavior of the entire organic motif on the silica surface. Such information is crucial, because the polar surface silanol groups might interact with the catalyst as well as the reactants, thus possibly altering the nucleophilicity of the DMAP motif and thereby the reaction yield.

Generally, thorough investigation of the pore space is necessary to gain a detailed picture of the environment in which heterogeneous catalytic reactions take place to allow for considerations concerning surface-substrate interactions and transport properties. To elucidate the pore space, a number of methods such as gas sorption, mercury intrusion porosimetry, microscopy and, to a lesser extent, 3D reconstruction through tomography are applied.[4] As such, numerous studies give insight into these aspects, showing how different pore sizes and shapes can affect the catalytic reaction taking place inside of the mesopore space.[5] Here, we perform in-depth physisorption analysis, especially applying Ar at $T = 87$ K.

With the colloidal Ludox silica nanoparticles, we have chosen a well-known, commercial non-porous catalyst support, to clarify the relevance of the mesopore space in general and whether the immobilization of the organocatalyst onto a silica carrier in itself already alters its reaction behavior and catalytic activity. To decouple this effect from the influence of a pore network, ideally a non-porous, flat silica substrate would have to be used for comparison. However, analysis of both the catalyst as well as the reaction products become unfeasible because of the very small amounts that can be immobilized on such a potential carrier material due to its inherently small surface area. This also holds true for non-porous particles in the micrometer range. As such, for this work, non-porous silica Ludox nanoparticles were chosen as a reference material, since the immobilized catalyst should still perform only on the outside of the particles without influence of pore confinement, while still offering sufficiently high surface areas through the size of the nanoparticles so that a reasonable amount of catalyst can be immobilized.

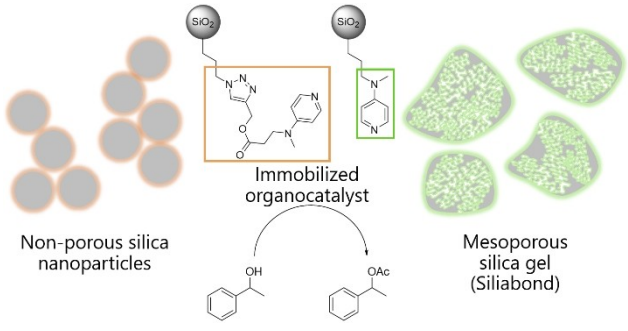

Figure 1. Schematic illustration of the two different materials used. The outer surface of the non-porous silica nanoparticles was functionalized with DMAP through an azide-alkine click reaction, while the commercial porous silica gel had the catalyst already immobilized in its mesopore network through a propyl-linker. Both materials were used for the catalytic acylation of 1-phenylethanol.

Results and Discussion

Characterization of the Materials

The SEM image (Figure 2, B) reveals the morphology of the material, showing particles with a large size distribution of 40–60 μm and varying shapes, edges and uneven surfaces. *Via* mercury intrusion porosimetry it was possible to confirm the mesoporosity of the material, showing a population of well accessible pores with the size of 4–12 nm and the absence of macropores (Figure 2, A). The larger "pores" ranging from 10 to 40 μm that can be seen in the pore size distribution are attributed to the interparticle voids that, because of the large particle size distribution, also vary to a larger degree. The mesopore space was further investigated *via* argon physisorption, with the isotherm shown in Figure 2(C) resembling a type IV isotherm as typical of mesoporous materials. The pore size distribution gained through the NLDFT method confirms the value of 6 nm given by the manufacturer for the average pore size, showing no presence of smaller micropores (Figure 2, D). However, it must be noted that the underlying fitting used for calculation shows considerable deviation from the measured curve in the lower relative pressure region (Figure S1, Supporting Information) due to the lack of suitable kernels available. This feature may also be the reason for the abrupt change of

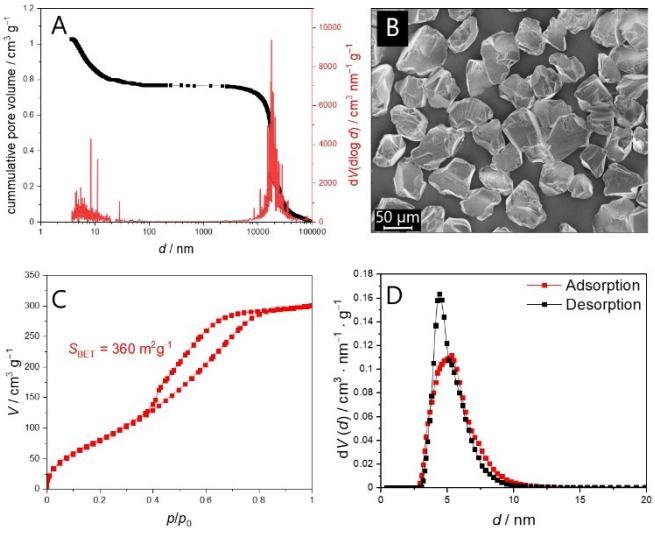

Figure 2. Characterization of the functionalized porous silica gel ("Siliabond"). Mercury intrusion porosimetry (A), scanning electron microscopy image (B), argon physisorption (87 K) isotherm (C) and corresponding NLDFT pore size distribution assuming a cylindrical pore geometry (D).

the pore size distribution at small values and the apparent absence of micropores.

Furthermore, when comparing the PSD based on either the adsorption or the desorption branch, it becomes apparent that negligible offset between the curves occurs. Concludingly, the emptying of the pores is not limited by smaller pores or pore necks, meaning the mesopores of the material are not restricted and that pore blocking can be excluded.

The organocatalyst DMAP is bound to the surface through a propyl linker as shown in Figure 1. A catalyst loading of 0.8 mmol g^{-1} was determined through elemental analysis based on the nitrogen content. For this work, the Siliabond silica gel was chosen deliberately because it offers a simpler and cheaper alternative to the highly specialized HPLC materials such as LiCrospher particles by Merck, which have been used in prior studies. One of the aims was to investigate if such complex materials are truly necessary for simple organic reactions or if less sophisticated carriers might suffice and make possible industrial applications more feasible. However, an initial concern was the lack of a uniform particle morphology and large size distribution which may give rise to an increasing pressure build up in flow setups. Thus, next to the Siliabond material we chose "Ludox" silica nanoparticles, which are quite uniform in size, but do not exhibit internal micro- or mesoporosity.

The here applied silica nanoparticles (Ludox TM40, 22 nm particle size) were shipped in an aqueous solution, but for the reaction with the organosilane, the particles had to be transferred to another solvent. Thus, transfer to methanol was performed through a series of centrifugation steps, gradually replacing the solvent until the refraction index of the supernatant matched that of methanol. Additionally, between functionalization steps, the particles had to be dried for analysis and later re-dispersed. The dispersions were analyzed using dynamic light scattering (DLS) and showed a broadened size distribution indicating agglomerates of several nanoparticles with an average hydrodynamic diameter d_h = 102 nm in methanol (Figure 3). After the first functionalization step, dispersing the nanoparticles already proved difficult, as very low weight-concentrations had to be used to prevent precipitation. Still, it was assumed that the comparably small agglomerates did not significantly hinder the click reaction with the organocatalyst in the second functionalization step (Figure 4). Since the catalysis itself could not be performed in methanol owing to the competing side reactions, the particles had to be transferred again to an aprotic solvent. Despite substantial effort, it was not possible to create stable dispersions of the final material in the tested solvents (DCM, acetonitrile, toluene), as precipitation was observed with each sample. The DLS measurements of the supernatant suggest strong polydispersity, with the larger agglomerates reaching sizes up to 630 nm. Therefore, although for the reaction rigorous stirring and strongly diluted dispersions were used, it has to be assumed that larger agglomerates consisting of anywhere up to nine nanoparticles might form during catalysis. The functionalization of the nanoparticles with the DMAP organocatalyst was carried out in a two-step procedure, involving the immobilization of an azide linker followed by a copper-catalyzed click reaction with the catalyst derivative (Figure 4). The progress was followed *via* diffuse reflectance infrared Fourier transform spectroscopy (DRIFT), revealing the appearance and subsequent reduction of the characteristic azide band at 2100 cm^{-1} indicating the successful immobilization of the linker and the catalyst, respectively. As seen in figure 5 the intensity of the azide band is diminished after the last reaction step, but has not disappeared entirely. This finding suggests that the reaction has not finished completely and remaining unreacted azide groups are still present on the silica surface. The final catalyst loading was determined using elemental analysis based on the nitrogen content of the sample and was calculated to be 0.1 mmol g^{-1}.

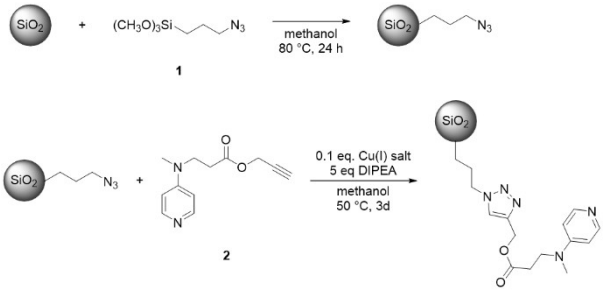

Figure 4. Functionalization route of the silica nanoparticles with the DMAP derivative.

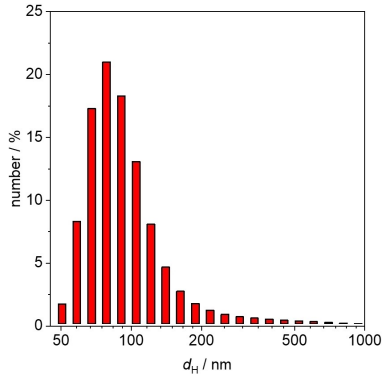

Figure 3. Particle size distribution of the silica nanoparticles in methanol based on DLS.

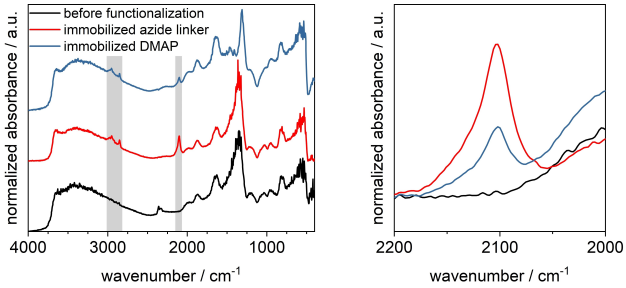

Figure 5. DRIFT spectra of the silica nanoparticles throughout the functionalization with the linker (red) and the organocatalyst (blue). Zoom on the characteristic azide band at ca. 2100 cm^{-1} (right).

Heterogeneous Catalysis

To compare the performance of the two materials, the acylation of 1-phenylethanol using acetic anhydride and triethylamine was chosen as model reaction, as comparable studies were performed previously in this group as well as reported in literature.[2] By using the Siliabond material in a batch setup (Figure 6), it was possible to reach near quantitative yields in a reaction time of only four hours. Reusing the material also showed no significant loss of activity, although the yield exceeding the 100% mark for the third cycle suggests product residues that falsely increase the detected amount of product. The existence of these product residues was confirmed by DRIFT and physisorption of the used material (Figure S2, Supporting Information), and is presumed to be caused by insufficient washing between reaction cycles. The functionalized silica Ludox nanoparticles on the other hand have shown to perform much worse, giving yields of only about 50% after 24 hours. While it was possible to achieve near quantitative conversion after 4 days, it is evident that the Ludox nanoparticles appear to be hindered in the effective catalysis of the acylation. It is likely that due to the aforementioned agglomeration and the accompanied formation of very small, diffusion-limited interparticle voids, the amount of active catalyst is reduced. Although the mesopores of the Siliabond material are relatively small, they appear to be more easily accessible for the substrates compared to the voids in-between the Ludox particles. As such, the spatial confinement in the former is presumed to be beneficial for the reaction, bringing together the substrates in close proximity to the catalytic sites and thus increasing the reaction rate substantially.

Because of the non-uniform morphology of the Siliabond material, the application in a flow reactor was expected to be problematic, due to a lower permeability compared to the materials being optimized for liquid chromatography, and the resulting high back pressures. However, surprisingly, the material could be packed into stainless steel columns and used in a flow setup, repeatedly exhibiting low back pressures of 1–3 bar only, depending on the flowrate. This way, the acylation of phenylethanol was performed in continuous flow, reaching high yields up to 90% even at 1 mL min^{-1} (Figure 7). In turn, the turnover frequency (TOF) of the material was calculated to 37 h^{-1} for the highest flowrate, which is in a comparable range to more complex, HPLC-optimized materials used in organocatalysis.[2] A comparison of the Siliabond packed bed flow reactor with a column packed with DMAP-functionalized LiCrospher® particles can be found in the supporting information (Figure S3). Here, a TOF value of 33 h^{-1} was reached with the highest flowrate (0.5 mL min^{-1}), which is only slightly higher than the value gained with the Siliabond column (23 h^{-1}).

To expand the scope of substrates, α-tocopherol was chosen as an industrially relevant compound, which is usually acylated to increase shelf-life.[6] In this case, the silica Ludox nanoparticles failed to yield any significant amount of product (Figure 8). While it was not possible to increase the amount of catalyst due to limitations of the material, the comparison with the mesoporous Siliabond particles shows that the latter performed significantly better in the acylation reaction, even with the same molar amount of catalyst present. As such, even with as little as 0.4 mol-% of catalyst, high yields of 88% could be reached in 3 hours, and quantitative yields after one day of reaction time. Apparently, the mesopores remain accessible

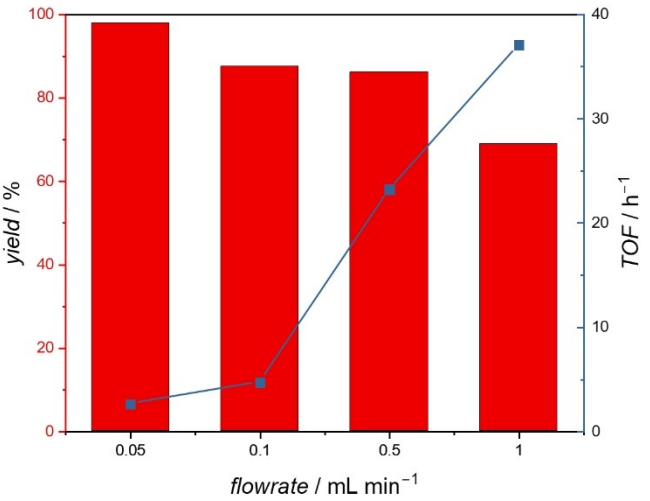

Figure 7. Yield of the acylation of 1-phenylethanol using the porous Siliabond silica gel in a packed bed reactor in continuous flow.

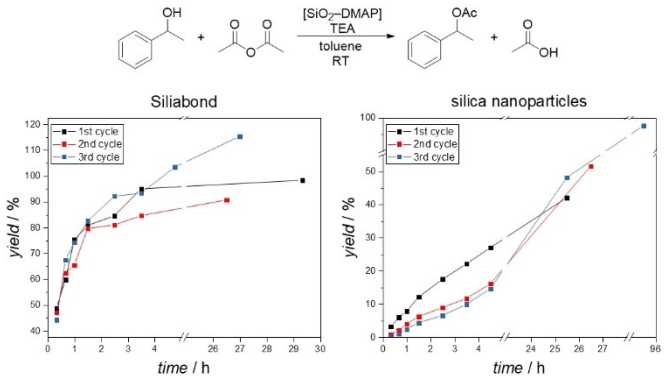

Figure 6. Yield of the catalytic acylation of 1-phenylethanol using 1 mol% of the DMAP-functionalized porous silica gel (left) and the non-porous silica nanoparticles (right) in a batch setup.

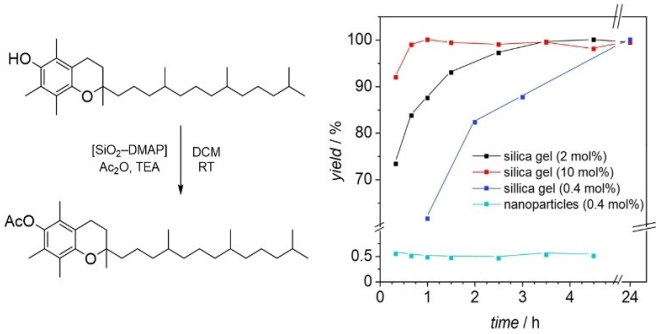

Figure 8. Yield of the acylation of tocopherol using the two different silica materials (Siliabond and Ludox particles) in a batch setup. For the porous silica gel, different catalyst loadings have been used.

even for the more sterically demanding substrate, and no significant diffusion limitation can be observed. On the other hand, the interparticle voids of the Ludox nanoparticles seem to be poorly accessible, presumably because the change of solvent causes the particles to agglomerate slightly stronger.

However, for an accurate comparison of the two materials, other factors have to be considered. Until now, the role of the linker used for anchoring the catalyst to the surface has hardly been discussed. Considering the substantial difference in the chemical nature as well as the size of the simple propyl group binding to the silica in the Siliabond material and the larger motif resulting from the click reaction used for the Ludox nanoparticles, a possible influence on the reaction yield cannot be neglected. As such, in another experiment, the bare Siliabond carrier material (commercially available as Sliliaflash by the same distributor) was functionalized in the present study through the same method as the Ludox nanoparticles. As described for Siliabond particles, the functionalization was monitored through DRIFT, although again, residual intensity of the azide band hints at an incomplete reaction, thus limiting the catalyst loading to 0.39 mmol g^{-1} (M1) and 0.26 mmol g^{-1} (M2) as given by elemental analysis. Thus, it was unfortunately not possible to reach similarly high loadings of organic moieties as for the Siliabond material (M3, 0.83 mmol g^{-1}). Additional physisorption analysis confirmed the successful immobilization, as each step was accompanied by a distinct decrease in pore volume (Figure 9). Still, the shape of the isotherms generally remains unchanged which indicates that the mesopore space remained intact and a homogeneous functionalization was achieved.

This material (M1 and M2), containing immobilized DMAP, but being connected by a different linker, was then tested alongside the Siliabond particles (M3) to assess possible differences in the catalytic performance.

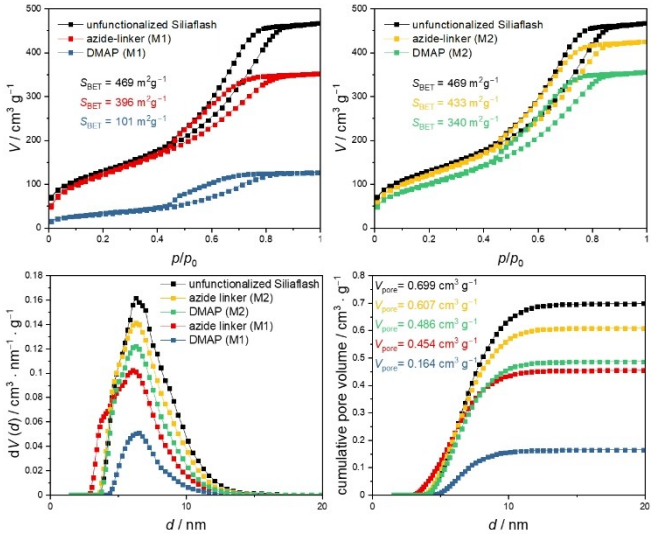

Figure 9. Nitrogen physisorption isotherms (top row), differential and cumulative pore size distributions and (NLDFT-based, bottom row) of the Siliaflash material before and after each functionalization step.

As seen in Figure 10 the newly functionalized material (blue and green line) has also proven active in the acylation of phenylethanol. Compared to the Siliabond material (black line) it even performed slightly better, as less time was needed to achieve similar yields. Possibly, the longer linker creates a larger distance to the polar silica surface, thus creating beneficial conditions for the reaction to occur. Indeed, it has been shown that the reaction is favored in less polar solvents, which is why in this work toluene was used.[7] Likewise, the polar silica surface might interfere with the ionic intermediates in a way that is detrimental to the reaction speed.

However, the comparison suffers from another parameter that needs to be considered: the catalyst loading. As it was not possible to recreate the same catalyst loading with the Siliaflash material, and the Siliabond could only be purchased with one particular loading, there is a large discrepancy in the catalyst loading among the samples. As such, the increase in catalytic activity might not stem from the different linker, but rather the lower catalyst loading, as these have already been shown to be beneficial in flow applications.[8] Presumably, a less crowded surface is favorable for the reaction to take place, which can also be observed when comparing the two Siliaflash samples, where the one with the lower loading (green line) performs slightly better.

To get a better understanding of how the catalyst motif behaves on and interacts with the silica surface, quantum chemical simulations of the surface structures in cluster approximations were performed. The presence of a pyridine group at the end of the ligand, which is known to show a high affinity towards forming hydrogen bonds with silanol groups, gives reason to assume the possibility of realizing at least two configurations in such systems: 1) the ligand is directed perpendicular to the surface; 2) the ligand forms a hydrogen bond between the silanol group of the silica surface and nitrogen of its pyridine ring.[9] Another question that arises when modeling such systems is the maximum degree of

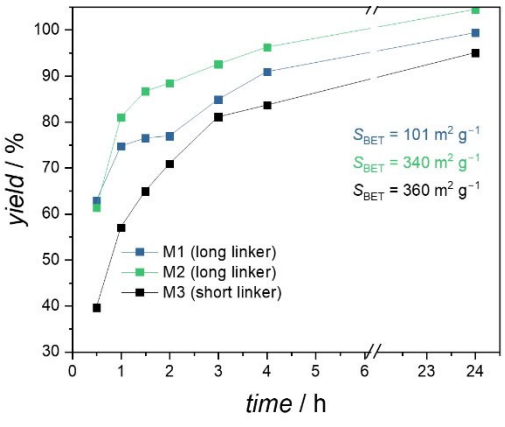

Figure 10. Yield in the acylation of 1-phenylethanol using the porous material functionalized with the short linker (M3, Siliabond, black curve) and the long linker (M1 and M2, Siliaflash, blue and green curve). Note that the loadings differ so drastically because the purchased material with the short linker could only be provided with the given loading which could unfortunately not be reached for the functionalized Siliaflash material with our method.

substitution of silanol groups and the influence of lateral interaction on the properties of long ligands. Therefore, an attempt is made to clarify these questions by means of quantum chemical modeling of surface structures in cluster approximation.

The surface of silica was modeled by clusters consisting of 6 and 16 silicon atoms (denoted as Si6-3 and Si-16, respectively), broken bonds were closed by silanol groups, and the spatial structure corresponded to the structure of beta-cristobalite, which most closely corresponds to the surface of amorphous silica.[10] During the grafting of the ligands, one more silicon atom (for each ligand) placed above the conventional surface appeared in the system. The first cluster (Figure 11, A) provides three long ligands to evaluate how the ligands interact with each other. The second cluster (Figure 11, B) provides for the possibility of an accurate conformation of the ligand with the formation of a hydrogen bond.

All calculations were performed by the restricted Hartree-Fock (RHF) method with the SBKJC valence basis set and the corresponding effective core potential, using the GAMESS software package.[11]

The optimal geometry of the Si6-3-DMAP model (Figure 11 A, bottom left) is characterized by an almost parallel arrangement of long ligands (at the same time, the chains are characterized by deformations with out-of-plane atoms). However, the distances between pyridine nitrogen atoms (7.28, 10.37, 12.41 Å) significantly exceed the distances between silicon atoms on the surface (5.22, 5.39, 5.71 Å). This means that

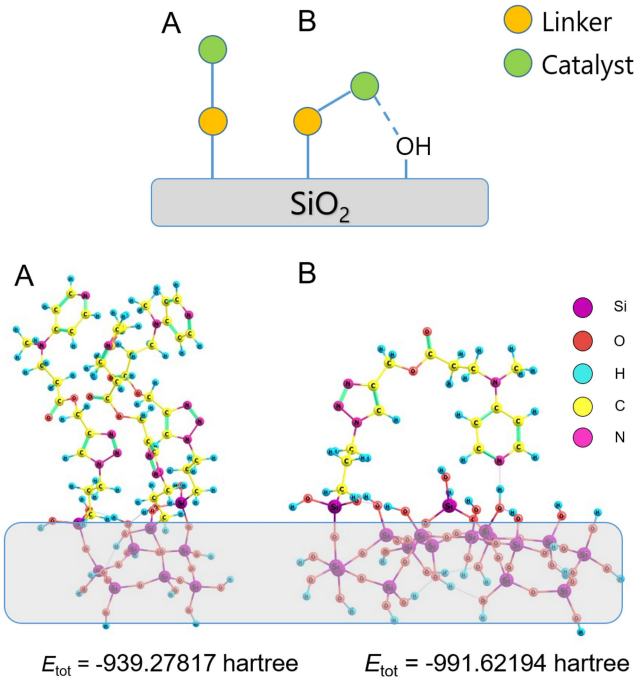

Figure 11. Schematic illustration of possible orientations of the organic catalyst and linker on the silica surface (top), and the models based on quantum chemical simulations (bottom). The catalyst is either oriented perpendicular to the surface, with an almost parallel arrangement between different linker chains (A) or is bend back to the surface (B) due to the formation of a hydrogen bond between the nitrogen atom of the pyridine moiety and a surface silanol group.

in the structure featuring complete substitution of hydroxyl groups, there is a significant repulsion between the ligands, which can significantly reduce the degree of substitution under the experimental conditions. This might be an explanation for not reaching similar loadings on the Siliaflash material with the longer linker, as compared to the shorter one present in the Siliabond material.

The optimized geometry of the Si-16 model (Figure 11 B, bottom right) corresponds to the formation of a 1.55 Å N…H–O hydrogen bond, with the H–O bond length increasing to 1.03 Å compared to 0.96 Å for free silanols, indicating a prominent acid–base interaction and hence a high probability of the existence of such structures. The conformation of the chain corresponds to the trans-cis-trans configuration of C–C–C links with the exit of the central part of the chain from the plane formed by the beginning and end of the chain.

The energy of the hydrogen bond was estimated using a quantum chemical calculation for a simplified model (Figure S4, Supporting Information) of the formation of an associate between orthosilicic acid and DMAP (initial) as an energy difference between free molecules and bonded by a hydrogen bond, and was found as $E_{H\text{-}bond} = -42.9\ kJ\,mol^{-1}$ at 298 K ($E_{H\text{-}bond} = -50.3\ kJ\,mol^{-1}$ at 0 K). Such a high value of the energy of the hydrogen bond indicates the sufficient strength of this bond, which determines the high probability of its formation on the surface. In addition, it should be noted that the energy of a hydrogen bond critically depends on its length (see above) and this once again confirms the high probability of its formation.

Similarly, for the short linker, two configurations are possible: the pyridine ring can form a hydrogen bond with the silanol group of the surface or is otherwise directed perpendicular to the surface (Figure S5, Supporting Information). Taking into account the values of the total energy for cluster models with a free and hydrogen-bonded pyridine group, it is possible to determine the hydrogen bond energy as their difference (−0.01166 hartree or $-30.6\ kJ\,mol^{-1}$). Such a value of the hydrogen bond energy is significantly lower than the calculated energy of the model hydrogen bond between DMAP and orthosilicate acid (−50.3 kJ/mol) and the calculated value of the hydrogen bond energy of the DMAP on long spacer (−71.2 kJ/mol). The low value of this energy for a ligand on a short spacer, despite its short length (1.524 Å), can be explained by significant stresses in the structure with a short spacer.

The existence of the hydrogen bond between catalyst and silica surface might constitute unfavorable conditions for the catalytic reaction, as the nitrogen atom of the pyridine ring plays the central role in its pathway: it has been shown that the first step of the acylation reaction is the formation of a ternary complex between DMAP, acetic anhydride and the alcohol, before the nucleophilic attack of the pyridine-ring nitrogen results in the formation of an acetylpyridinium cation under expulsion of an acetate leaving group. However, the catalytic data (Figure 10) do not support this hypothesis, since the longer linker, for which the hydrogen bond is more likely to appear, performs even slightly better. Still, the differences in activity might stem from varying surface loadings. Possibly, the closer orientation of the catalyst to the polar silica surface in case of

the short linker might be disadvantageous to the above-mentioned mechanism. Indeed, end-capping of the remaining silanol groups with hexamethyldisilazane slightly increased the yield, suggesting that hydrogen bonding with silanol groups might interact with the catalytic motif. (see Supporting Information, Figure S6).

It has to be noted that the influence of the base triethylamine, which is present in the reaction mixture was neglected in the quantum chemical simulations. Not only might the base compete with the pyridine moiety of the catalyst to form hydrogen bonds to the surface, it might also deprotonate the silanol groups due to the considerable difference of their pK_a values (10.7 for triethylamine and 2–7 for silanol groups). Because of the difficulties to account for this in the calculations, especially considering the range of pK_a given for surface silanol groups in literature, this has been omitted in the current work.[12]

Activation Energy

To further investigate potential differences between the different linker molecules, the kinetic properties of the different materials can be compared, especially with our previous work on DMAP-functionalized silica.[3] Therein, the reaction order and activation energy of the heterogeneously catalyzed acylation of phenylethanol, using a DMAP-functionalized silica monolith, was determined through a series of experiments with different temperatures and reaction times (controlled through the flow rate in a flow reactor). This way, it could be shown that while the reaction order was identical to that of the homogeneous reaction, the activation energy was reduced, probably due to the unique environment created by the polar silica surface and the non-polar solvent as well as the close contact of substrate and catalyst in the heterogeneous reaction.[2,7,13] Figure 12 shows the product concentration of the acylation of phenylethanol at room temperature as a function of time, using a packed bed column reactor filled with Siliabond-DMAP. Using only reaction times below 10 s to stay within the range of microkinetics, it was possible to determine the initial reaction rate v in a set of experiments at different temperatures (Figure S7, Supporting Information). Following Equation (1) the reaction rate coefficients k were calculated, as the reaction was previously shown to follow a first-order behavior using a surplus of acetic anhydride. With these and Equation (2), a linearized Arrhenius plot (Figure 12, right) allowed for the determination of the activation energy E_A giving a value of 7.3 ± 1.3 kJ mol^{-1}.

$$v = k \cdot c(PE) \cdot c(Ac_2O) \quad (1)$$

$$\ln(k) = \ln(A) - \frac{E_A}{R} \cdot \frac{1}{T} \quad (2)$$

This value is close to what was found for the DMAP-functionalized silica monolith previously.[3] Taking into account potential inaccuracies such as the reaction time being affected by fluctuations in the flow rate, the activation energies gained through this method remain an approximation and bear uncertainties on the order of 2 kJ/mol. Still, on the one hand, this value confirms the significantly lowered activation energy compared to the homogenous reaction as calculated by Xu et al.[7] On the other hand, it also shows that, the influence of using the different linker molecules appears to be negligible.

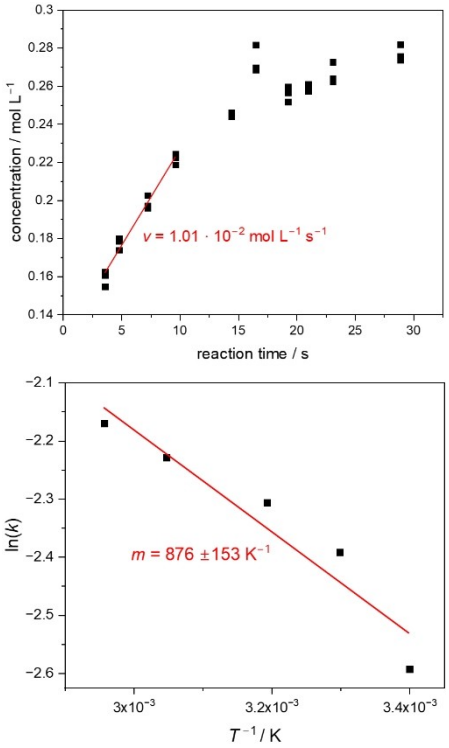

Figure 12. Determination of the initial reaction rate for the reaction at room temperature (top) and Arrhenius plot for different temperatures (bottom).

Conclusions

The present study intended to advance in using a versatile organocatalyst, 4-(dimethylamino)pyridine (DMAP), being covalently linked to porous silica materials, for efficient catalysis of fundamental organic reactions (here: acylations) in liquid media, especially in flow. Previous studies had already shown that this concept provides both, high yields and stable catalytic performance. Yet, the porous silica materials used (commercial packedbed particles and monolithic silica) are specially designed with respect to the mesopore space as well as optimized flow properties. They are commercialized for HPLC, but suffer from elaborate synthesis and comparably high costs.[3] Based on this initial study, here two other types of commercialized silica particles were employed to address basics questions in heterogeneous organocatalysis exemplified for DMAP: on the one hand we studied the impact of covalently linking the DMAP motif to a silica surface, supported by quantum-chemical calculations. On the other hand, we aimed at elucidating the relevance of a mesoporous network as well as the importance

of a well-defined particle shape, for instance in relation to commercial packed-bed particles used for HPLC.

Thus, DMAP-functionalized silica Ludox nanoparticles, possessing no internal nanoporosity, were compared to commercial mesoporous DMAP-functionalized silica particles (Siliabond-DMAP) in the catalytic acylation of two different compounds, i.e. phenylethanol and α-tocopherol. This way, it could be shown that, on the one hand, the catalysis using the Ludox nanoparticles is generally feasible. Although the reaction times required were much higher compared to mesoporous Siliabond-DMAP, it was possible to achieve near quantitative yields after three days. Conclusively, the catalyst does not suffer from inherent deactivation through the immobilization on a silica surface. On the other hand, the mesoporous Siliabond material enabled much higher product yields with short reaction times, reaching similar catalytic performance as the previously used DMAP-functionalized materials.[3] The data suggest that the reasonable catalytic performance is due to the beneficial effect of a continuous mesopore network, a high surface area and a sufficiently large mesopore diameter (mean pore size ca. 6 nm). While this result seems intuitive at first, this study now offers empirical proof through decoupling the relevance of a mesopore network from the immobilization itself. However, one must keep in mind that the silica nanoparticles showed significant agglomeration which limits the amount of active, accessible catalyst as well and creates "pore-like" spaces through interparticle voids. This result indicates that the catalytic performance of DMAP-functionalized silica is mainly determined by the mesospore space and mass transport limitations, rather than possible unfavorable interaction of the DMAP motif with or on the silica surface, at least for moderate loadings.

Additionally, the commercial Siliabond material in general proved to be efficient not only in the batch catalysis but also in a packed bed reactor used in a continuous flow setup. Interestingly, the performance was similar to the previously utilized silica materials (commercial micrometer-sized particles and monoliths, both used for HPLC), indicating that the irregular shape of the commercial Siliabond particles does not significantly impede the catalytic performance in flow, at least for the flow rates studied. As such, it constitutes a cheaper, but promising commercial material that is competitive with more specialized and complex alternatives such as HPLC-optimized spherical particles or silica monoliths.

Lastly, the role of the dimension of the catalyst linker was investigated for the Siliabond-type materials, by using two linkers differing in length, i.e. the formal distance of the DMAP motif from the silica surface. It could be shown that both linkers perform similarly well and the activation energies as determined through kinetic studies were almost identical. Quantum chemical calculation suggest that for the longer linker motif, containing the azide moiety, interaction of the pyridinium unit with the the silanol groups might be relevant, possibly impeding the first step in the catalytic mechanism. Interestingly, the calculations also revealed substantial steric constraints between the linker molecules, assuming complete substitution of the -OH groups. These insights point to a possible explanation for our experimental observation that the maximum loading with linker and, concomitantly, the catalyst remains significantly below the theoretical loading, based on the surface area. Yet, these findings show that the performance of immobilized DMAP seems to be largely uninfluenced by the linker moiety.

In conclusion, our study shows that commercial silica particles featuring a more irregular particle shape, i.e. of the Siliabond type, exhibit efficient catalytic performance using the versatile DMAP organocatalyst, even if performed in flow. These results therefore may contribute to lay the basis for expanding the usage of immobilized DMAP and similar organocatalysts in heterogeneous organocatalysis.

Experimental Section

Functionalization of the Siliaflash Particles with the Azide-Linker

0.500 g of the silica particles were dried under vacuum at 80 °C overnight. Then, 10 mL of dry toluene, 327 μL (1.78 mmol, 1 eq.) or 32.7 μL (0.18 mmol, 0.1 eq.) depending on the desired loading, were added alongside with 248 μL (1.78 mmol, 1 eq.) or 24.8 μL (0.18 mmol, 0.1 eq.) of Triethylamine. The suspension was then stirred under argon at 80 °C for approximately 24 hours. Afterwards, the solution was separated by centrifugation and the particles were washed with toluene, dichloromethane, methanol, and a 1:1 mixture of methanol and water. After drying at 40 °C under vacuum, a colorless powder was obtained.

Functionalization of the Siliaflash Particles with DMAP

0.200 g of the azide-functionalized silica particles were suspended in 15 mL toluene. Depending on the azide loading, three equivalents of the DMAP precursor (0.157 g, 0.720 mmol or 0.051 g, 0.234 mmol), two equivalents of DIPEA (84 μL, 0.482 mmol or 27 μL, 0.155 mmol) and the tip of a spatula of bromotris(triphenylphosphine)copper(I) ($CuBr(PPh_3)_3$) were added. The suspension was then stirred at 50 °C for three days. Afterwards the material was washed with acetonitrile, 5 *w*-% aqueous EDTA solution (until the supernatant solution appeared colorless) water and methanol to get rid of residual copper species. After drying under vacuum at 40 °C, a yellow-brown powder was obtained. HRMS (ESI-TOF): $[M+Na]^+$ calculated for $C_{12}H_{14}N_2O_2$: m/z = 241.0948; found: m/z = 241.0947

Synthesis of 3-(Azidopropyl)trimethoxysilane (1, Figure 4)

5.284 g (81.3 mmol) sodium azide and 0.604 g (1.64 mmol) tetrabutylammonium iodide were dried overnight under vacuum. Both were suspended in 40 mL acetonitrile under argon and 3 mL of (3-chloropropyl)trimethoxysilane was added before stirring at 90 °C for five days. Afterwards, the suspension was filtrated and the solvent removed under reduced pressure. The crude product was dissolved in dry pentane and solid residues again removed by filtration. The process was repeated several times until no solid residues precipitated and a colorless liquid was obtained. **^{1}H-NMR** (400 MHz, CDCl3): δ (ppm) = 3,57 (s, 9H, RSi(OCH3)3, 3,26 (t, 2H, R-CH2-N3), 1,71 (p, 2H, R-CH2-CH2-N3), 0,69 (t, 2H, Si-CH2-R)

Synthesis of the DMAP Precursor (2, Figure 4)

0.254 g (2.34 mmol) of 4-(methylamino) pyridine was added to 1 mL (9.05 mmol) of propargyl acrylate and stirred at 90 °C for three and a half hours. After removing excess propargyl acrylate via vacuum distilliation, the crude product was purified through a silica gel flash chromatography (DCM/Methanol 9:1) and a yellow solid was obtained.

Functionalization of the Silica Nanoparticles with the Azide Linker

The aqueous silica nanoparticle dispersion was diluted to 10 w-% through dropwise addition of methanol and sonicated until no phase separation or precipitate was observable. After centrifugation, the supernatant transparent phase was replaced with methanol and the process was repeated seven times. Afterwards, the solvent was removed slowly using a rotary evaporator and the nanoparticles were dried under vacuum at 40 °C overnight.

For the functionalization, 1.172 g (approx. 0.90 mmol of surface silanol groups)[14] of the nanoparticles were again heated under vacuum at 80 °C and then dispersed in 20 mL of dry methanol. After addition of 164.4 μL (0.895 mmol, 1 eq.) of the azide linker **1** and 124.8 μL (0.895 mmol, 1 eq.) triethylamine, the dispersion was stirred for 24 h at 50 °C. Then, most of the solvent was removed by centrifugation, the nanoparticles washed with methanol three times (50 mL total) and, after removing the solvent with a rotary evaporator, dried under vacuum at 40 °C to give 0.789 g of functionalized nanoparticles.

Functionalization of the Silica Nanoparticles with DMAP

For the second step in the functionalization scheme, 0.256 g (0.0266 mmol of azide based on elemental analysis) of the azide-functionalized nanoparticles were dispersed in 190 mL of methanol and stirred together with 0.0625 g (0.287 mmol) of the DMAP precursor **2**, 0.0066 g (0.0071 mmol) $CuBr(PPh_3)_3$ and 680.7 μL (4.003 mmol) of N–N-diisopropylethylamine for three days at 50 °C.

Batch catalysis of the Acylation Of 1-Phenylethanol

For the batch catalysis of the acylation of 1-phenylethanol using either material, a stock solution of 363 μL (3.03 mmol, 1 eq.) 1-phenylethanol, 627 μL (4.50 mmol, 1.5 eq.) triethylamine and 425 μL (4.50 mmol, 1.5 eq.) acetic anhydride in 10 mL toluene was prepared. Then, either 14.5 mg of the Siliabond material or 120 mg of the functionalized nanoparticles were added, which equals 1 mol% of DMAP in respect to the substrate 1-phenylethanol. The reaction mixture was stirred at room temperature and periodically stopped for centrifugation to prepare samples for gas chromatography of the supernatant solution to monitor the product yield. Before each recycling experiment, the silica material was washed with toluene, DCM, methanol and a methanol water mixture (1:1).

Flow catalysis of the Acylation of 1-Phenylethanol with a Siliabond Packed Bed Reactor

For the flow catalysis, the Siliabond material was packed into stainless steel columns and attached to an HPLC pump to be used as packed bed reactors in a flow setup. The stock solution was prepared similarly to the batch catalysis and pumped through the reactor with a flowrate of 0.05 to 1.0 mL min^{-1}. The solution exiting the reactor was collected periodically to prepare samples for gas chromatography to monitor the product yield.

For the kinetic study, the packed bed reactor was placed in a column oven set to the specific temperatures at least 30 minutes before starting the reactions. The flowrates ranged from 1.0 mL min^{-1} to 8.0 mL min^{-1} to allow for short reaction times.

Batch catalysis of the Acylation Of α-Tocopherol

For the batch catalysis of the acylation of α-tocopherol using either material, a stock solution of 0.866 g (2.01 mmol) of tocopherol, 560 μL triethylamine and 486 μL acetic anhydride in 20 mL DCM was prepared. Then, varying amounts of either the Siliabond material or the nanoparticles were added, depending on the catalyst loading that was aimed for (0.4 mol%, 2 mol%, 10 mol%). The reaction mixture was stirred at room temperature and periodically stopped for centrifugation to prepare samples for HPLC analysis of the supernatant solution to monitor the product yield. Before each recycling experiment, the silica material was washed with DCM, methanol and a methanol water mixture (1:1).

Characterization Methods

Argon physisorption experiments were performed using an "Autosorb iQ" instrument by Quantachrome Instruments at a temperature of 87 K using a CryoSync cryostat. Pore size distributions were calculated using an NLDFT kernel (Ar at 87 K, zeolites/silica, cylindrical pores, adsorption branch) provided by the Quantochrome software ASiQwin.

Nitrogen physisorption experiments were performed using a "Quadrasorb evo" by Quantachrome Instruments at a temperature of 77 K. Pore size distributions were calculated using an NLDFT kernel (N2 at 77 K on silica, cyldinrical pores, adsorption branch) provided by the Quantachrome software ASiQwin.

Mercury intrusion porosimetry was performed using a Pascal 140 and 440 porosimeter by Thermo Fisher Scientific in a pressure range of 0–400 mPa.

For scanning electron microscopy, the sample was sputter coated with platinum and measured with a Zeiss Merlin (acceleration voltage of 2.00 kV, current of 113 pA).

A CHN-analyzer Flash EA-1112 (Thermo Scientific) was used for Elemental Analysis

HPLC measurements were performed using a Dionex P680 pump equipped with a Degasys DG2410 Degasser and a Dionex UVD170 U detector for separation. A Eurospher II CN column was used with a solvent mixture of 97% hexane and 3% iso-propanol and a flowrate of 1.0 mL min^{-1}.

Acknowledgements

Open Access funding enabled and organized by Projekt DEAL.

Conflict of Interests

The authors declare no conflict of interest.

Data Availability Statement

The data that support the findings of this study are available from the corresponding author upon reasonable request.

Keywords: Mesoporous silica materials · Organocatalysis · Continuous flow catalysis · Supported catalysis

[1] a) A. El Kadib, R. Chimenton, A. Sachse, F. Fajula, A. Galarneau, B. Coq, *Angewandte Chemie* **2009**, *48*, 4969–4972; b) K. Turke, R. Meinusch, P. Cop, E. Da Prates Costa, R. D. Brand, A. Henss, P. R. Schreiner, B. M. Smarsly, *ACS Omega* **2021**, *6*, 425–437; c) R. D. Brand, S. A. Busche, H. G. Börner, B. M. Smarsly, *ChemCatChem* **2023**, *15*; d) Y. Arakawa, H. Wennemers, *ChemSusChem* **2013**, *6*, 242–245; e) M. Gruttadauria, F. Giacalone, R. Noto, *Chemical Society reviews* **2008**, *37*, 1666–1688; f) A. F. Trindade, P. M. P. Gois, C. A. M. Afonso, *Chemical reviews* **2009**, *109*, 418–514; g) B. Clapham, T. S. Reger, K. D. Janda, *Tetrahedron* **2001**, *57*, 4637–4662; h) J. G. Hernández, E. Juaristi, *Chemical communications (Cambridge, England)* **2012**, *48*, 5396–5409; i) O. Sánchez-Antonio, K. A. Romero-Sedglach, E. C. Vázquez-Orta, E. Juaristi, *Molecules (Basel, Switzerland)* **2020**, *25*; j) M. Ferré, R. Pleixats, M. Wong Chi Man, X. Cattoën, *Green Chem.* **2016**, *18*, 881–922; k) D. Das, G. Pathak, S. L. Rokhum, *RSC Adv.* **2016**, *6*, 104154–104163.

[2] J. S. Schulze, R. D. Brand, J. G. C. Hering, L. M. Riegger, P. R. Schreiner, B. M. Smarsly, *ChemCatChem* **2022**, *14*, e202101845.

[3] a) A. R. Bogdan, B. P. Mason, K. T. Sylvester, D. T. McQuade, *Angewandte Chemie* **2007**, *46*, 1698–1701; b) V. D'Elia, Y. Liu, H. Zipse, *Eur J Org Chem* **2011**, *2011*, 1527–1533; c) V. Pandarus, G. Gingras, F. Béland, R. Ciriminna, M. Pagliaro, *Catal. Sci. Technol.* **2011**, *1*, 1600; d) R. A. T. Verdier, J. H. Mikkelsen, A. T. Lindhardt, *Org. Process Res. Dev.* **2018**, *22*, 1524–1533.

[4] a) M. Thommes, K. Kaneko, A. V. Neimark, J. P. Olivier, F. Rodriguez-Reinoso, J. Rouquerol, K. S. Sing, *Pure and Applied Chemistry* **2015**, *87*, 1051–1069; b) D. Stoeckel, C. Kübel, M. O. Loeh, B. M. Smarsly, U. Tallarek, *Langmuir : the ACS journal of surfaces and colloids* **2015**, *31*, 7391–7400.

[5] a) T. Das, H. Uyama, M. Nandi, *New J. Chem.* **2018**, *42*, 6416–6426; b) H. Kraus, J. Rybka, A. Höltzel, N. Trebel, U. Tallarek, N. Hansen, *Molecular Simulation* **2021**, *47*, 306–316.

[6] T. Zhang, B. Li, X. Zhang, J. Wang, L. Wei, B. Zhao, B. Li, *J Porous Mater* **2020**, *27*, 1639–1648.

[7] S. Xu, I. Held, B. Kempf, H. Mayr, W. Steglich, H. Zipse, *Chemistry (Weinheim an der Bergstrasse, Germany)* **2005**, *11*, 4751–4757.

[8] J. S. Schulze, J. Migenda, M. Becker, S. M. M. Schuler, R. C. Wende, P. R. Schreiner, B. M. Smarsly, *J. Mater. Chem. A* **2020**, *8*, 4107–4117.

[9] M. R. Alves, et al., *J Porous Mater* **2021**, *28*, 323–335.

[10] A. Rimola, D. Costa, M. Sodupe, J.-F. Lambert, P. Ugliengo, *Chemical reviews* **2013**, *113*, 4216–4313.

[11] G. M. J. Barca, et al., *The Journal of chemical physics* **2020**, *152*, 154102.

[12] M. O. Onizhuk, A. V. Panteleimonov, Y. V. Kholin, V. V. Ivanov, *J Struct Chem* **2018**, *59*, 261–271.

[13] C. P. Haas, T. Müllner, R. Kohns, D. Enke, U. Tallarek, *React. Chem. Eng.* **2017**, *2*, 498–511.

[14] L. T. Zhuravlev, *Colloids and Surfaces A: Physicochemical and Engineering Aspects* **2000**, *173*, 1–38.

Manuscript received: October 1, 2024
Revised manuscript received: November 17, 2024
Accepted manuscript online: November 19, 2024
Version of record online: December 11, 2024